Revista de Informática Teórica e Aplicada - RITA - ISSN 2175-2745
Vol. 31, Num. 1 (2025) 26-32

RESEARCH ARTICLE

Application of Denoising Diffusion Probabilistic Methods in Fetal MRI

Aplicação de Métodos Probabilísticos de Difusão para Remoção de Ruído em Imagens Fetais de Ressonância Magnética

Ana Cláudia Souza Vidal de Negreiros[1]*, Gilson Giraldi[2], Heron Werner[3]

Abstract: Magnetic resonance imaging (MRI) is a common type of medical image acquisition that can also be used to diagnose early diseases. In this sense, fetal MRI is a non-invasive method to generate high-quality fetal volumes and to perform important clinical analysis. However, image denoising is necessary in many situations to ensure accurate evaluations. Thus, approaches such as Denoising Diffusion Probabilistic Methods (DDPM) have emerged and reached great results in this kind of task. In this work, we applied two DDPM-based approaches (an original and an improved one) besides two self-supervised deep models in a fetal MRI dataset. The results showed that, for the used fetal MRI dataset, the improved DDPM, named I-DDPM outperformed the counterparts considering two evaluation metrics for image quality, the Peak Signal-to-Noise Ratio (PSNR) and Root Mean Squared Error (RMSE).
Keywords: Image Denoising — DDPM-Based Approaches — Medical Area — Fetal MRI

Resumo: A ressonância magnética (MRI) é um tipo comum de aquisição de imagem médica que também pode ser usada para diagnosticar doenças precoces. Nesse sentido, o MRI fetal é um método não invasivo para gerar volumes fetais de alta qualidade e realizar análises clínicas importantes. No entanto, a remoção de ruído nas imagens é necessária em muitas situações para garantir avaliações precisas. Assim, abordagens como os Métodos Probabilísticos de Difusão para Redução de Ruído (DDPM) surgiram e alcançaram ótimos resultados nesse tipo de tarefa. Neste trabalho, aplicamos duas abordagens baseadas em DDPM (uma original e uma aprimorada), além de dois modelos profundos auto-supervisionados em um conjunto de dados de MRI fetal. Os resultados mostraram que, para o conjunto de dados de MRI fetal utilizado, o DDPM aprimorado, denominado I-DDPM, superou os demais considerando duas métricas de avaliação da qualidade da imagem, o Peak Signal-to-Noise Ratio (PSNR) e o Erro Quadrático Médio (RMSE).
Palavras-Chave: Remoção de ruído — Abordagens baseadas em DDPM — Área médica — MRI fetal

[1] *Federal Rural University of the Semi-Arid (UFERSA), Brazil*
[2] *National Laboratory for Cientific Computing (LNCC), Brazil*
[3] *Biodesign Lab Dasa, Pontifical Catholic University of Rio de Janeiro (PUCRJ), Brazil*
***Corresponding author**: anaclaudia.negreiros@ufersa.edu.br
DOI: http://dx.doi.org/10.22456/2175-2745.143785 • **Received:** 04/11/2024 • **Accepted:** 02/12/2024

1. Introduction

Advances in image processing happen continuously with remarkable results been published every day. In the specific case of image denoising, the scientific community realized how necessary to improve image analysis in areas like security-related (e.g., identification of wanted people), environmental management (e.g., oil spill detection), and health prevention (e.g., disease detection in early stages).

In this sense, recently, Diffusion Models have played an essential role in this area. Specifically, denoising diffusion probabilistic models (DDPM), originally proposed by Ho et al. [1], has emerged as a new machine learning approach with the capability to learn from data distributions and synthesize high-quality images, outperforming well-known classical methods [2], [3], [4].

A DDPM model is based on two simple steps: (1) the forward process involves gradually introducing Gaussian noise to an input image until the image converges to an isotropic Gaussian distribution or a completely noise image; (2) the reverse denoising process entails progressively eliminating noise from an initially noisy distribution until the genuine underlying data is revealed, resulting in a coherent image. In this way, the method learns how to convert a completely

(Gaussian) noise image into a coherent one. Formally, DDPM is a distribution learning-based method, that tries to transform a Gaussian distribution by performing iterative refinements [3]. Besides, DDPM can effectively leverage the entire data distribution while preserving crucial imaging features [2].

Among other tasks, DDPM has also been applied for image denoising. In general, the recent literature has shown that considering the image denoising task, it also can outperform well-known methods such as Generative Adversarial Networks (GANs) and Variational Auto-Encoders (VAEs) [5], [6]. This fact encourages newly developed works in this direction. In this sense, recently, DDPM has been applied for specific kinds of images, such as fetal magnetic resonance imaging (MRI) [7] mostly to improve image quality due to the goal of early disease diagnosis to fetal imagery that can be crucial for child health [8], [9].

Taking this into consideration, this work will apply two DDPM approaches and two self-supervised models in a fetal MRI dataset. The first one is the original DDPM (O-DDPM) proposed by Ho et al. [1], the second one is the improved DDPM (I-DDPM) introduced by Nichol and Dhariwal [10], the third is a self-supervised deep learning method, named N2N, developed by Lehtine et al. [11] and the last one is another self-supervised technique, called N2V, proposed by Krull et al. [12]. In this context, the main contribution of this work is that we will analyze those methods in a specific fetal MRI dataset for the first time. Besides, works that applied DDPM in fetal MRI are rare in the literature, highlighting this work's importance. Another contribution of this work is that we performed comparison with results of the reference [13].

The rest of this paper is organized as follows. Section II brings the recent related works that were performed or proposed methods based on DDPM. Section III presents the used MRI fetal image dataset. Section IV addresses original and improved DDPM approaches. Section V details and compares the results obtained by applying both DDPM approaches. Finally, Section VI concludes the work with the main results and ideas for future research.

2. Related Works

Recently, many works based on DDPM have been developed aiming to address different tasks. The work developed by [2] proposed a framework for generating high-resolution magnetic resonance imaging (MRI) from low resolution counterparts, improving the uncertainty of denoising diffusion probabilistic models (DDPM). Muller-Franzes et al. [14] compared DDPM with GANs for recovering contrast-enhanced breast MRI, and the DDPM results outperformed GANs, according to radiologists. The reference [3] developed a DDPM-based approach that tried to transform a normal distribution into a specific data distribution based on iterative refinements. Their application was for PET image denoising. In [4] authors built a DDPM using 2D brain images trained using slices in which health tissue was cropped out and is learned to be inpainted again, aiming to make enable the automatic analysis of images feature lesions, and further downstream tasks. The work [15] proposed a conditional DDPM translation from the cone-beam computed tomography (CBCT) to the computed tomography (CT) distribution for the image quality improvement of CBCT. Authors used a time-embedded U-Net architecture with residual and attention blocks to gradually transform the Gaussian noise sample to the target CT distribution conditioned on the CBCT. In [5] it is investigated the velocity of convergence with lower and higher timesteps in denoising tasks with diffusion models. Lyu et al. [16] adapted DDPM to learn the probability distribution of high-dimensional raw data and reconstructed the microstructures of many composite materials. Browne et al. [6] developed a DDPM to predict super-resolution pathology slide images from low resolution inputs. Mueller [17] proposed an attention-enhanced conditioning-guided DDPM approach for synthesizing additional machine fault diagnosis training data. Sui et al. [18] incorporated into Remote Sensing (RS) Single Image Super-Resolution (SISR) a DDPM to generate Super-Resolution (SR) images with enhanced textural details. Li et al. [19] presented feature map denoising model based on DDPM for feature refinement. In the case of fetal images, the work developed by [20] applied DDPM in the context of anomaly detection fetal brain ultrasound, presenting a novel unsupervised model for this task.

3. Dataset

In this research, we used a fetal MRI dataset, generated from 38 different patients (pregnant). The dataset used in this work is not available to the public. For the image generation, a $1.5-T$ scanner (Magnetom Aera, Siemens, Erlangen, Germany) performed the MRI examination, with the surface coil placed on the abdomen. It was applied a 3D T2-weighted true fast imaging sequence with steady-state precession (truefisp) in sagittal plane ($TR/TE = 3.02/1.43ms$); besides, following isotropic voxel ($1.0 \times 1.0 \times 1.0mm^3$); matrix: $256 \times 256mm^2$, 136 slices, with a total acquisition time of $26s$. Also, maternal sedation was not used in the patients because it is unnecessary in this data collection.

Besides, to acquire the MRI dataset, the pregnant was positioned in dorsal or left lateral decubitus, with the feet entering the magnet first. Then, the images were acquired using a controlled setup with image obtained during maternal breath-hold to produce high-quality images with minor levels of artifacts/noise. During the capture of fetal MRI, it is not possible to prevent the movement of the fetus. So, it is not guaranteed that images obtained in a controlled environment will be free of artifacts due to fetal movements [13].

For this work, synthetic images were generated to compose the pairs of images (clean and noisy ones). In this context, the additive Gaussian noise [21] was applied to the clean images. The additive Gaussian noise is widely used in many contexts. Thus, Fig. 1 shows two pairs of clean and noisy fetal images. The clean one (ground truth) is from our dataset described above, and the noisy one was generated by additive

Gaussian noise with standard deviation $\sigma = 20$.

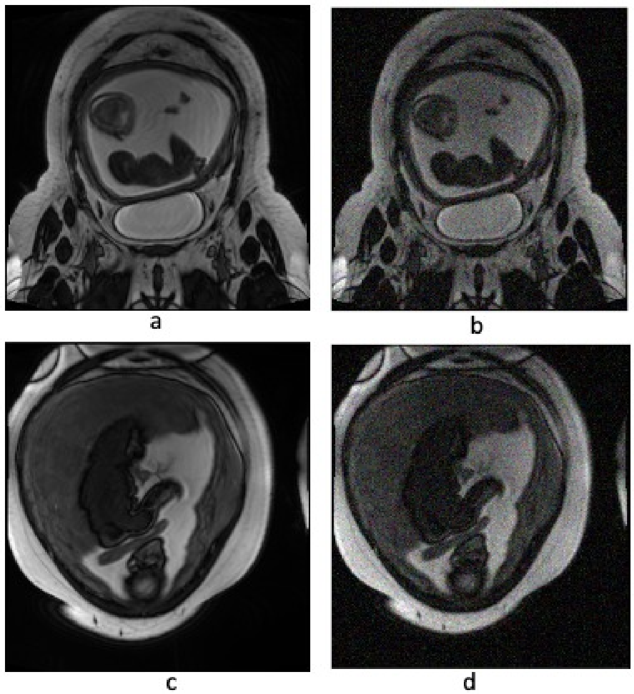

Figure 1. (a) Ground truth image 1. (b) Noisy image correspondent to ground truth image 1. (c) Ground truth image 2. (d). Noisy image correspondent to ground truth image 2.

4. Denoising Diffusion Probabilistic Model

The forward process in diffusion models is performed to progressively destroy all the information in the image in a sequence of timesteps T where each stage adds Gaussian noise into the input image. Then, a neural network learns a reverse of this process (denoising process) where effectively the noise is removed step by step. Thus, assume the target data $x_0 \sim q(x_0)$. Thereby, in more details, over this called forward process, it is possible to define a Markov diffusion process q that adds Gaussian noise to x_0 in each step, which can be written as [1]

$$q(x_1,\ldots,x_T|x_0) = \prod_{t=1}^{T} q(x_t|x_{t-1}), \tag{1}$$

$$q(x_t|x_{t-1}) = \mathcal{N}(x_t; \sqrt{1-\beta_t}\, x_{t-1}, \beta_t \mathbf{I}). \tag{2}$$

One property of the forward process q was that it allowed us to sample at any arbitrary stage directly conditioned on x_0. Denoting $\alpha_t = 1-\beta_t$ and $\bar{\alpha}_t = \prod_{l=1}^{t} \alpha_l$, we could have

$$q(x_t|x_0) = \mathcal{N}(x_t; \sqrt{\bar{\alpha}_t}\, x_0, (1-\bar{\alpha}_t)\mathbf{I}), \tag{3}$$

$$x_t = \sqrt{\bar{\alpha}_t}\, x_0 + \sqrt{1-\bar{\alpha}_t}\, \varepsilon, \tag{4}$$

where $\varepsilon \sim \mathcal{N}(0,\mathbf{I})$. Based on Bayes theorem, the posterior also followed Gaussian distribution,

$$q(x_{t-1}|x_t) = \mathcal{N}\left(x_{t-1}; \tilde{\mu}_t(x_t,x_0), \frac{1-\bar{\alpha}_{t-1}}{1-\bar{\alpha}_t}\beta_t \mathbf{I}\right), \tag{5}$$

with

$$\tilde{\mu}_t(x_t,x_0) = \frac{\sqrt{\bar{\alpha}_{t-1}}\beta_t}{1-\bar{\alpha}_t}x_0 + \frac{\sqrt{\bar{\alpha}_t(1-\alpha_{t-1})}}{1-\alpha_t}x_t. \tag{6}$$

If we intended to sample from the goal data distribution $q(x_0)$, we could first sample from $q(x_T)$, which was an isotropic Gaussian distribution given a large enough T. Hereafter, based on the posterior distribution $q(x_{t-1}|x_t)$, we could obtain sample of x_0. Nevertheless, $q(x_{t-1}|x_t)$ was not computable as the distribution of x_0 was unknown. The DDPM framework tried to approximate $q(x_{t-1}|x_t)$ by $p_\theta(x_{t-1}|x_t)$ through a network with parameter θ, where

$$p_\theta(x_{t-1}|x_t) = \mathcal{N}(x_{t-1}; \tilde{\mu}_\theta(x_t,t), \sigma_t^2\mathbf{I}). \tag{7}$$

Instead of directly approximating $\tilde{\mu}_\theta(x_t,t)$ by a neural network, Ho et al. [1] proposed to approximate the noise ε in Eq. 4 by a network as $\varepsilon_\theta(x_t,t)$ which could also be interpreted as the gradient of the data log-likelihood, known as the score function. Based on Eqs. 4 and 6, $\tilde{\mu}_\theta(x_t,t)$ could be expressed as

$$\tilde{\mu}_\theta(x_t,t) = \frac{1}{\sqrt{\alpha_t}}\left[x_t - \frac{\beta_t}{\sqrt{1-\bar{\alpha}_t}}\varepsilon_\theta(x_t,t)\right]. \tag{8}$$

Based on trained score function $\hat{\varepsilon}_\theta(x_t,t)$, and Eqs. 7 and 8, each improvement step during inference was

$$x_{t-1} = \frac{1}{\sqrt{\alpha_t}}\left[x_t - \frac{\beta_t}{\sqrt{1-\bar{\alpha}_t}}\hat{\varepsilon}_\theta(x_t,t)\right] + \sigma_t z_t, \tag{9}$$

where $z \sim \mathcal{N}(0,\mathbf{I})$.

The whole process demonstrated above corresponds to the original DDPM. However, the improved DDPM proposed by [10] performed some changes in the process aiming better results. Thus, they proposed a learnable variance in the process by using the following equation

$$\sum_\theta(x_t,t) = \exp\left(v \log\beta_t + (1-v)\tilde{\beta}_t\right). \tag{10}$$

Furthermore, [10] proposed a hybrid loss, which is defined by following equation

$$L_{\text{hybrid}} = L_{\text{simple}} + \lambda L_{\text{vlb}}, \tag{11}$$

where

$$L_{\text{simple}} = \mathbb{E}_{(t,x_0,\varepsilon)}\left[\|\varepsilon - \varepsilon_\theta(x_t,t)\|^2\right]. \tag{12}$$

Also, L_{simple} doesn't depend on $\sum_\theta(x_t,t)$ and given that according to [22] the combination of q and p is a variational auto-encoder, the variational lower bound (vlb) can be written as

$$L_{\text{vlb}} := L_0 + L_1 + \cdots + L_{T-1} + L_T. \tag{13}$$

Aside from L_0, each term of Eq. 13 is a KL divergence between two Gaussians and can be evaluated in closed form. However, to evaluate L_0 for images it is assumed that each color component is divided into 256 bins, thus it is possible to compute the probability of $p_\theta(x_0|x_1)$ landing in the correct bin (which is tractable using the cumulative distribution function of the Gaussian distribution).

They also set $\lambda = 0.001$ to prevent L_{vlb} from dominating L_{simple}. The authors experimented that because they believed it could improve the results compared to original DDPM. Also, a third proposed improvement by [10] was the use of a cosine schedule instead a linear noise schedule, which was proposed in terms of $\bar{\alpha}_t$:

$$\bar{\alpha}_t = \frac{f(t)}{f(0)}, \tag{14}$$

where

$$f(t) = \cos\left(\left(\frac{t}{T} + s\right)\frac{\pi}{2(1+s)}\right)^2. \tag{15}$$

Besides, they used a small offset s to prevent β_t from being too small near $t = 0$, since they found that having very small amounts of noise at the beginning of the process made it hard for the network to predict ε accurately enough. These are the main improvements proposed by [10].

5. Comparisons and Discussion Results

The dataset used in this work (described in Section III) contains 2590 image pairs (original, noisy), where 80% were used for training, 10% for validation, and 10% as the test set. We ran the codes in Python, using PyTorch [23] for I-DDPM, O-DDPM, and N2N. Also, we used TensorFlow [24] and Keras [25] for N2V. The codes for O-DDPM, I-DDPM, N2N, and N2V can be found in [1], [10], [11] and [12], respectively. Also, in this work, the network weights were initialized according to those references. Thus, for the diffusion-based methods, they initialized the training using ADAM (Adaptative Moment Estimation) [26] with the optimizer function with parameters $\beta = 0.8$ and $\beta = 0.9$ and $\varepsilon = 10^{-8}$, and a learning rate of 0.00001, with batch size 64. The two DDPM-based models were trained using 2000 epochs and 300 timesteps. Also, the code was run in a GPU Tesla T4 with 16GB of GDDR6 memory and 2560 CUDA cores.

First, we applied both O-DDPM and I-DDPM to perform results comparisons. Thus, in both DDPM processes occurs the forward process (Eq. 2), where the input image is destroyed step by step by adding Gaussian noise in each iteration.

One of the purposes at the end of the forward process and the beginning of the backward process (denoising process) is to predict the noise distribution accurately. This stage is important and necessary to undo the noise-adding operation. Thus, at the beginning of the backward process, the predicted noise is away from the ground truth noises. However, this is natural because the network is still learning the patterns and the results improve over the training epochs.

In this sense, the network learns the ground truth noise over training. At this point, it is possible to undo this noise addition and denoise the corrupted image (x_t). Fig. 2 shows that the predicted noises are initially away from the added noise. On the other hand, over the epochs training, the tendency is that the predicted noise approximates the ground truth noise (Fig. 3).

After the denoising process, the outcome is the denoised image. Fig. 4 shows one image from the test set that were denoised using both original and improved DDPM. To apply DDPM approaches, we used as input the noise image (x_0) such as in [13], which were images corrupted by a Gaussian noise using $\sigma = 20$ (standard deviation). In this sense, unfortunately, by visual analysis, it is hard to see and conclude what model performed better. However, in this work, we also computed some quality image metrics to compare the results, *PSNR* and *RMSE*.

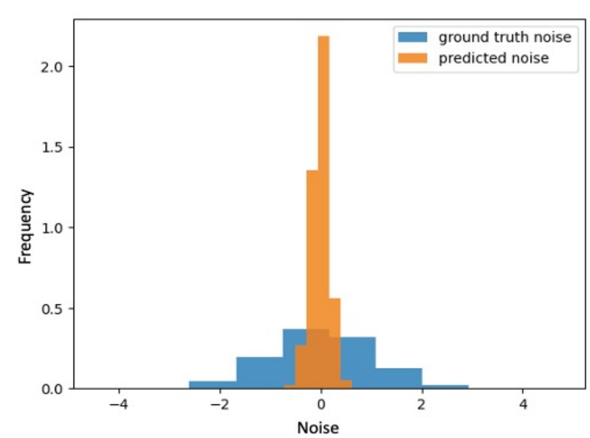

Figure 2. Ground truth and predicted distribution noise at the beginning of the backward training process.

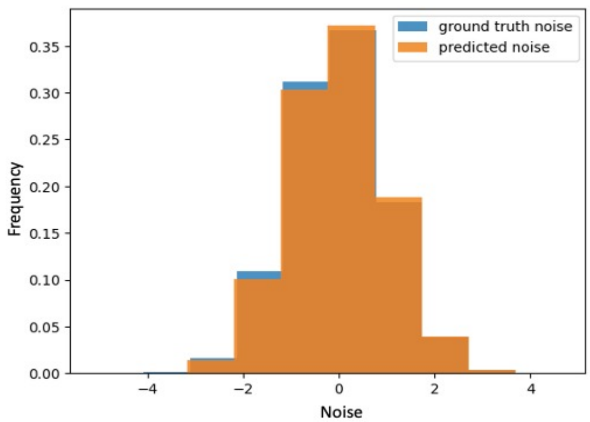

Figure 3. Ground truth and predicted distribution noise at the end of the backward training process.

In this context, we used widely quality image metrics, *PSNR*, and *RMSE*, to evaluate the results of both approaches. The formulas to compute these image quality metrics are given below.

$$\mathrm{PSNR} = 20\log(\mathrm{MAX}_I) - 10\log(\mathrm{MSE}). \tag{16}$$

In the above formula, MAX_I represent the maximum pixel value of image I and MSE (Eq. 17) is the mean squared error that considers the "true" numeric values for comparison between actual and degraded image [27]

$$\mathrm{MSE} = \frac{1}{M \times N} \sum_{i=1}^{M} \sum_{j=1}^{N} [g(i,j) - f(i,j)]^2, \tag{17}$$

where M and N are the pixel amounts in the x direction and y direction, respectively, of the thin section images. Also, $g(i,j)$ and $f(i,j)$ are the grey values of the original (ground truth) thin section image and the cleaned thin section image, respectively, at point (i,j).

The *RMSE*, another quality measure used in this paper, is defined as

$$\mathrm{RMSE}(g,f) = \sqrt{\mathrm{MSE}}, \tag{18}$$

where MSE was defined in Eq. (17), g is the original signal, and f is the denoised signal.

Table 1 summarizes the quantitative results of both DDPM methods and, for comparison purposes, it also presents the results achieved by N2N and N2V self-supervised methods, reported in [13]. This table presents the image quality metrics (*PSNR* and *RMSE*), in terms of the mean over the test set composed by 259 images, for the four methods (O-DDPM, I-DDPM, N2N, N2V).

In general, quality image metrics are widely used because the quantitative results are very important and essential to make accurate conclusions about the results. In this case, Table 1 informs that, even with the lack of visual perception, improved DDPM outperforms the counterparts O-DDPM, N2V and N2N, since for this method, *PSNR* is greater than others and the *RMSE* is the smallest one. Thus, considering the tested dataset and the added Gaussian noise, I-DDPM is recommended for the denoising image problem. However, in terms of training required time, these approaches have no significant variations.

Table 1. Results for O-DDPM, I-DDPM, N2N, and N2V methods considering the fetal test set and mean values of *PSNR* and *RMSE* metrics

Methods		
	PSNR	*RMSE*
O-DDPM	31.2376	0.0231
I-DDPM	33.4562	0.0087
N2N	31.1867	0.0261
N2V	29.3456	0.0342

In Fig. 4 it isn't possible to visually identify differences between the denoised images (Fig. 4.(c) and Fig. 4.(d)), i.e. I-DDPM and O-DDPM performed very similarly, although the first one was quantitatively better. However, it is possible to see the difference between the ground truth Fig. 4.(a) and the denoised images Fig. 4.(c) and Fig. 4.(d). Thus, it means that there is a place to have better results considering the clean image. In this sense, other methods and techniques must continue to be applied aiming for better results.

Besides, we also performed a test using images with a higher level of Gaussian noise ($\sigma = 30$). The idea was to verify the performances of both the I-DDPM and the O-DDPM. The output was a *PSNR* of 30.3476 for the I-DDPM and a *PSNR* of 29.7858 for the O-DDPM. Also, the *RMSE* for the I-DDPM was 0.0156 and the *RMSE* for O-DDPM was 0.0298. Thus, this test endorses the results shown in Table 1, where the I-DDPM was the best technique for the used dataset. Fig, 5 shows the visual results for this test.

6. Conclusions

This work aimed to apply two DDPM-based approaches (O-DDPM and I-DDPM) and compare the results with two self-supervised methods, N2N and N2V. We used these methods in fetal MRI aiming to perform denoising tasks to improve the clinical analyses of this kind of image. The cleaner the medical image the greater the probability to detect problems and perform prevention attitudes.

Considering the two applied DDPM-based methods, the I-DDPM performed better compared with the counterparts O-DDPM, N2V, and N2N, using the same dataset and under the same training conditions. Indeed, the improved approach achieved greater results, presenting a bigger *PSNR* and a smaller *RMSE* compared to the other three methods. In this sense, the objective of this work was achieved and the

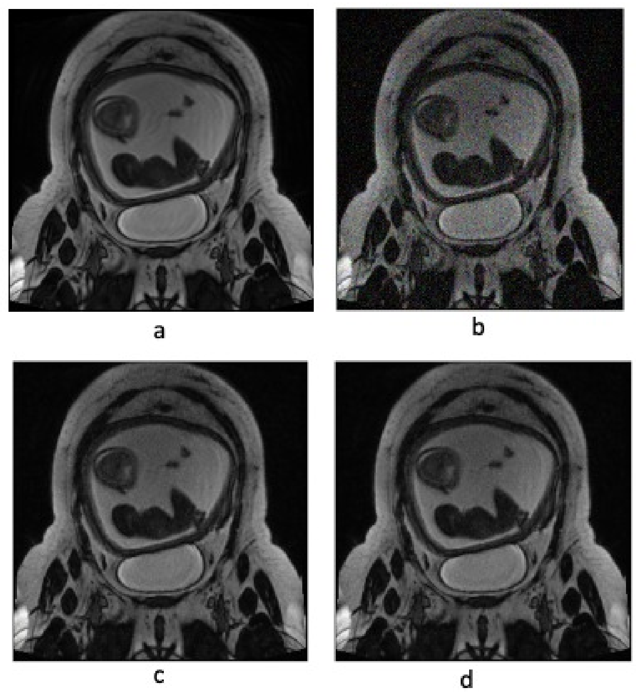

Figure 4. (a) Ground truth. (b) Noisy image. (c) Denoised image obtained by the O-DDPM method. (d) Denoised image obtained by the I-DDPM approach.

contribution was confirmed.

Some of the limitations in developing this article include using a private dataset that is not very large, consisting of 2,590 images. Additionally, we could not compare our results with more methods because, in general, it is challenging to find the code implementations for image denoising methods.

For future works, we intend to improve the denoising task in fetal MRI and test these methods by applying more noise levels. Thus, we will try other denoising methods and perform results benchmarking. Also, we intend to propose improving the DDPM approach to reach better results and use real fetal images. This improvement consists of applying a complex probabilistic distribution (q-Exponential model) to try to predict the noise and perform noise reduction or complete elimination based on this probabilistic model. Besides, we will test other fetal datasets, and different kinds of images, such as ultrasonography imagery.

Acknowledgements

The authors would like to thank FAPERJ ("Fundação Carlos Chagas Filho de Amparo à Pesquisa do Estado do Rio de Janeiro") for funding this paper (Financing Code E-26/200.640/2023 (284828)). The study involving fetal MRI was approved by the DASA ethics committee. All patients involved signed a consent form approving the use of the images used in this research.

Author contributions

Ana Cláudia Souza Vidal de Negreiros: Conceptualization, Methodology, Investigation, Validation, Writing - Review and Editing. Gilson Giraldi: Methodology, Validation, Writing - Review and Editing. Heron Werner: Writing - Review.

References

[1] HO, J.; JAIN, A.; ABBEEL, P. Denoising diffusion probabilistic models. *Advances in neural information processing systems*, v. 33, p. 6840–6851, 2020.

[2] CHANG, C.-W. et al. High-resolution mri synthesis using a data-driven framework with denoising diffusion probabilistic modeling. *Physics in Medicine & Biology*, IOP Publishing, v. 69, n. 4, p. 045001, 2024.

[3] GONG, K. et al. Pet image denoising based on denoising diffusion probabilistic model. *European Journal of Nuclear Medicine and Molecular Imaging*, Springer, v. 51, n. 2, p. 358–368, 2024.

[4] DURRER, A.; CATTIN, P. C.; WOLLEB, J. Denoising diffusion models for inpainting of healthy brain tissue. *arXiv preprint arXiv:2402.17307*, 2024.

[5] KIM, J.-Y. et al. Denoising task difficulty-based curriculum for training diffusion models. *arXiv preprint arXiv:2403.10348*, 2024.

[6] BROWNE, A. W. et al. Deep learning assisted imaging methods to facilitate access to ophthalmic telepathology. *Ophthalmology Science*, Elsevier, v. 4, n. 3, p. 100450, 2024.

[7] ZHANG, M. et al. Fetaldiffusion: Pose-controllable 3d fetal mri synthesis with conditional diffusion model. *arXiv preprint arXiv:2404.00132*, 2024.

[8] DASH, D.; KUMAR, M. An ensemble-based stage-prediction machine learning approach for classifying fetal disease. *Healthcare Analytics*, Elsevier, v. 5, p. 100322, 2024.

[9] UNGUREANU, A. et al. Learning deep architectures for the interpretation of first-trimester fetal echocardiography (life)-a study protocol for developing an automated intelligent decision support system for early fetal echocardiography. *BMC Pregnancy and Childbirth*, Springer, v. 23, n. 1, p. 20, 2023.

[10] NICHOL, A. Q.; DHARIWAL, P. Improved denoising diffusion probabilistic models. In: PMLR. *International conference on machine learning*. [S.l.], 2021. p. 8162–8171.

[11] LEHTINEN, J. et al. Noise2noise: Learning image restoration without clean data (2018). *arXiv preprint arXiv:1803.04189*, 1803.

[12] KRULL, A.; BUCHHOLZ, T.-O.; JUG, F. Noise2void-learning denoising from single noisy images. In: *Proceedings of the IEEE/CVF conference on computer vision and pattern recognition*. [S.l.: s.n.], 2019. p. 2129–2137.

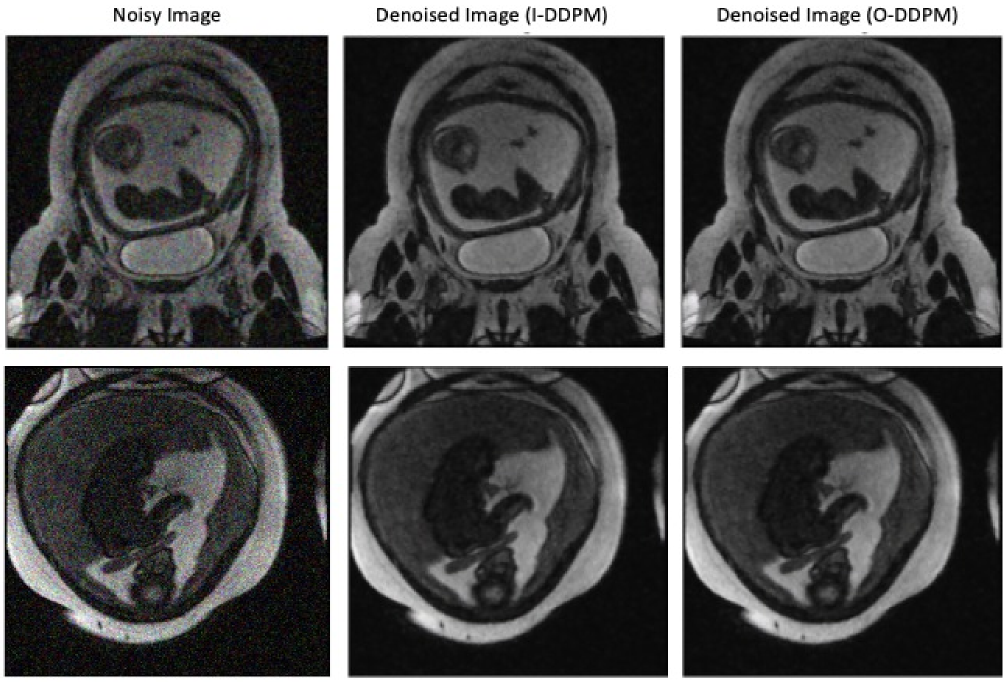

Figure 5. Test using a higher level of the Gaussian noise ($\sigma = 30$).

[13] NEGREIROS, A. C. S. V. de et al. Self-supervised image denoising methods: an application in fetal mri. In: SBC. *Anais do XVIII Workshop de Visão Computacional*. [S.l.], 2023. p. 137–141.

[14] MÜLLER-FRANZES, G. et al. Diffusion probabilistic versus generative adversarial models to reduce contrast agent dose in breast mri. *European Radiology Experimental*, Springer, v. 8, n. 1, p. 53, 2024.

[15] PENG, J. et al. Cbct-based synthetic ct image generation using conditional denoising diffusion probabilistic model. *Medical physics*, Wiley Online Library, v. 51, n. 3, p. 1847–1859, 2024.

[16] LYU, X.; REN, X. Microstructure reconstruction of 2d/3d random materials via diffusion-based deep generative models. *Scientific Reports*, Nature Publishing Group UK London, v. 14, n. 1, p. 5041, 2024.

[17] MUELLER, P. N. Attention-enhanced conditional-diffusion-based data synthesis for data augmentation in machine fault diagnosis. *Engineering Applications of Artificial Intelligence*, Elsevier, v. 131, p. 107696, 2024.

[18] SUI, J.; WU, Q.; PUN, M.-O. Denoising diffusion probabilistic model with adversarial learning for remote sensing super-resolution. *Remote Sensing*, MDPI, v. 16, n. 7, p. 1219, 2024.

[19] LI, G. et al. A generic plug & play diffusion-based denosing module for medical image segmentation. *Neural Networks*, Elsevier, v. 172, p. 106096, 2024.

[20] MYKULA, H. et al. Diffusion models for unsupervised anomaly detection in fetal brain ultrasound. In: SPRINGER. *International Workshop on Advances in Simplifying Medical Ultrasound*. [S.l.], 2024. p. 220–230.

[21] KHMAG, A. Additive gaussian noise removal based on generative adversarial network model and semi-soft thresholding approach. *Multimedia Tools and Applications*, Springer, v. 82, n. 5, p. 7757–7777, 2023.

[22] KINGMA, D. P. Auto-encoding variational bayes. *arXiv preprint arXiv:1312.6114*, 2013.

[23] PASZKE, A. et al. Pytorch: An imperative style, high-performance deep learning library. *Advances in neural information processing systems*, v. 32, 2019.

[24] ABADI, M. et al. Tensorflow: Large-scale machine learning on heterogeneous distributed systems. *arXiv preprint arXiv:1603.04467*, 2016.

[25] KETKAR, N. *Introduction to keras*. [S.l.]: Springer, 2017.

[26] KINGMA, D. P. Adam: A method for stochastic optimization. *arXiv preprint arXiv:1412.6980*, 2014.

[27] SHAH, A. et al. Comparative analysis of median filter and its variants for removal of impulse noise from gray scale images. *Journal of King Saud University-Computer and Information Sciences*, Elsevier, v. 34, n. 3, p. 505–519, 2022.